remote sensing

MDPI

Article

Application of LISA Gravitational Reference Sensor Hardware to Future Intersatellite Geodesy Missions

William Joseph Weber [1,2,*], Daniele Bortoluzzi [2,3], Paolo Bosetti [3], Gabriel Consolini [1], Rita Dolesi [1,2] and Stefano Vitale [1,2]

[1] Dipartimento di Fisica, Università di Trento, Via Sommarive 14, 38123 Trento, Italy; gabriel.consolini@studenti.unitn.it (G.C.); rita.dolesi@unitn.it (R.D.); stefano.vitale@unitn.it (S.V.)
[2] Trento Institute for Fundamental Physics and Applications/INFN, Via Sommarive 9, 38123 Trento, Italy; daniele.bortoluzzi@unitn.it
[3] Dipartimento di Ingegneria Industriale, Università di Trento, Via Sommarive 9, 38123 Trento, Italy; paolo.bosetti@unitn.it
* Correspondence: williamjoseph.weber@unitn.it

Abstract: Like gravitational wave detection, inter-spacecraft geodesy is a measurement of gravitational tidal accelerations deforming a constellation of two or more orbiting reference test masses (TM). The LISA TM system requires TM in free fall with residual stray accelerations approaching the $\mathrm{fm/s^2/Hz^{1/2}}$ level in the mHz band, as demonstrated in the LISA Pathfinder "Einstein's geodesic explorer" mission. Current geodesy missions are limited by accelerometers with 100 $\mathrm{pm/s^2/Hz^{1/2}}$ level, due to intrinsic design limitations, as well as the challenging low Earth orbit environment and operating conditions. A reduction in the TM acceleration noise could lead to an important improvement in the scientific return of future geodesy missions focusing on mass change, especially in a scenario with multiple pairs of geodesy satellites. We present here a preliminary assessment of how the LISA TM system, known as the "gravitational reference sensor" (GRS), could be adapted for use in future geodesy missions aiming at residual TM accelerations noise at the $\mathrm{pm/s^2/Hz^{1/2}}$ level, addressing the major design issues and performance limitations. We find that such a performance is possible in a geodesy GRS that is simpler and smaller than that used for LISA, with a lighter, sub-kg TM and gaps reduced from 4 mm to less than 1 mm. Acceleration noise performance limitations will likely be closely tied to the required levels of applied actuation forces on the TM.

Keywords: gravitational reference sensor; geodesic motion

Citation: Weber, W.J.; Bortoluzzi, D.; Bosetti, P.; Consolini, G.; Dolesi, R.; Vitale, S. Application of LISA Gravitational Reference Sensor Hardware to Future Intersatellite Geodesy Missions. *Remote Sens.* **2022**, *14*, 3092. https://doi.org/10.3390/rs14133092

Academic Editors: Luca Massotti and David N. Wiese

Received: 11 May 2022
Accepted: 23 June 2022
Published: 27 June 2022

1. Introduction

LISA, the Laser Interferometer Space Antenna [1], is the ESA Cosmic Vision L3 "Large Mission" and aims to be the first orbiting detector of gravitational waves, observing in the 100 μHz–1 Hz band and currently under preparation for launch in the 2035 timeframe. It employs a constellation of three spacecraft, forming a triangle with side length $L = 2.5$ million km, each containing two free-falling test masses (TM) as geodesic references to trace the tidal force produced by a passing gravitational wave, which is then measured by laser interferometry along the three arms of the constellation. The LISA sensitivity at low frequencies, below 4 mHz, is limited by stray TM accelerations, with a noise requirement $S_g < 3\,\mathrm{fm/s^2/Hz^{1/2}}$, relaxed below 0.4 mHz.

This required performance has been demonstrated by the ESA mission LISA Pathfinder (LPF), which achieved a differential acceleration noise floor between two LISA TM below 2 $\mathrm{fm/s^2/Hz^{1/2}}$ between 1 and 10 mHz (10 $\mathrm{fm/s^2/Hz^{1/2}}$ at 0.1 mHz) [2,3], in a drag-free spacecraft control with applied TM forces below the 100 $\mathrm{pm/s^2}$ level. The "gravitational reference sensor" (GRS) employed in LISA Pathfinder [4,5]—the TM itself and the surrounding hardware serving as Faraday shield, capacitive sensor and electrostatic actuator—is thus

flight-tested hardware at the heart of the LISA measurement, crucial to the low frequency "super massive black hole" science promised by the mission.

An intersatellite geodesy mission like GRACE-FO [6,7] is essentially a short single-arm LISA in low Earth orbit ($h \approx 500$ km), using laser interferometry to detect the varying gravitational tidal acceleration—in this case from spatial and temporal variations of the terrestrial Newtonian field—between two geodesic reference TM at a distance $L \approx 200$ km. The TM are the inertial elements of electrostatic accelerometers, with performance at the level of 100 pm/s^2/Hz$^{1/2}$ residual acceleration noise, with noise power increasing as f^{-1} below 5 mHz [8].

This paper addresses the possibility of adapting LISA-like GRS hardware for use in improving the sensitivity of future geodesy missions addressing spatial-temporal variations of terrestrial gravity and mass change. The objective would be to improve the gravitational tidal acceleration measurement sensitivity by a factor 100, into the pm/s^2 regime with the LISA GRS sensor modified for the "easier" geodesy acceleration noise requirements but also for the harsher conditions and specific needs of a mission in low Earth orbit.

The roughly five orders of magnitude jump achieved in going from a GRACE accelerometer to the fm/s^2 LISA Pathfinder TM performance required a very different TM system, moving from a 70 g TM with a discharge wire and roughly 100 μm TM-electrode gaps [9] to a nearly 2 kg TM with several mm gaps and no electrical/mechanical connection to the surrounding electrode housing (EH), in addition to the use of spacecraft drag-free control. These changes were costly in size, mass and complexity. The goal here is to broadly address the design changes necessary to improve geodesy sensitivity by a factor 100 with the simplest and smallest GRS system possible, considering also the impact of the trade between a drag-free system and accelerometry.

The relatively simple considerations presented here, applying our LISA and LISA Pathinder experience to several key performance driving design parameters for the TM and electrode housing, serve as a starting point for a future study in Italy adapting our LISA design heritage into a complete geodesy GRS system. A more advanced study is ongoing in NASA[10], reaching further into a full implementation including the electronics and needed mechanisms, as well as an overall analysis of the mission geodesy performance. Our findings however are quite similar, in the rough design numbers and in the general conclusion: that a LISA-like GRS, made smaller and optimized for terrestrial orbits can indeed allow a large leap in geodesy metrology performance, most completely if there is some compensation, even partial, of the spacecraft drag.

2. Rationale and Possible Top-Level Requirements for a Geodesy Gravitational Reference Sensor

The motivation for improving the TM system for a future geodesy mission is fairly straightforward: with the introduction of interspacecraft laser interferometry in GRACE-FO [7], measurement sensitivity is limited at all useful frequencies by the test mass (TM) acceleration noise. Considering a GRACE-like measurement as a one-arm interferometric measurement—described in Appendix A—of the differential gravitational acceleration Δg between free-falling reference masses along the axis x that joins them, we find

$$S_{\Delta g} \approx 2S_g + \frac{1}{2}\omega^4\left(S_{x_{SC}} + 2L^2 S_{\Delta\nu/\nu}\right) + 2\left|\omega^2 - \omega_{xx}^2\right|^2 S_{x_{TM}} \quad (1)$$

where we include:

- S_g, the PSD of single TM stray acceleration noise;
- $S_{x_{SC}}$, interferometry displacement noise in a "one-way" link measurement between the two spacecraft (SC);
- $S_{x_{TM}}$, the measurement noise in the local SC-TM displacement measurement;
- $S_{\Delta\nu/\nu}$, relative noise in the laser frequency.

We separate the laser frequency noise term from the remaining inter-SC measurement noise $S_{x_{SC}}$—shot noise, phase-meter noise, etc.—for its dominant role in a single arm

interferometry measurement. We note that the local TM position readout noise $S_{x_{TM}}$ couples into the measurement of Δg both as an effective displacement metrology term and through the static force gradient or "stiffness" (per unit mass), ω_{xx}^2, coupling the relative SC-TM jitter into TM acceleration.

Equation (1) is valid independently of whether the TM is forced to follow the SC—accelerometer operation—or is an unforced, free-falling reference for SC "drag-free" control. However, the extraction of the differential gravitational measurement is different (see Appendix A), and the presence of significant x axis TM force actuation, as needed in accelerometer operation, can be a dominant contributor to both the acceleration noise S_g and to the stiffness ω_{xx}^2.

Figure 1 compares a model of GRACE-FO performance with the improved differential acceleration sensitivity achievable with a GRS TM system. For GRACE-FO we take as reference values a TM acceleration noise of 100 pm/s^2/Hz$^{1/2}$ [8] and laser frequency noise of 6×10^{-14} /Hz$^{1/2}$ $\times \left(\frac{1\,\mathrm{mHz}}{f}\right)^{1.2}$, as deduced from Refs. [7,8]. The laser frequency noise gives an equivalent one-way link displacement noise around 15 nm/Hz$^{1/2}$ at 1 mHz and 1 nm/Hz$^{1/2}$ at 100 mHz [7]. The sensitivity is limited at all frequencies below 40 mHz by TM acceleration noise. This is compared to the projected performance achieved with a TM at 1 pm/s^2/Hz$^{1/2}$ acceleration noise performance, along with contributions from the TM readout noise (to be discussed in the following sections). This improves the sensitivity by a factor 100 at lower frequencies and leaves the sensitivity in the 1–100 mHz band interferometry-limited.

A rough illustration of the increase in sensitivity for a single pass over a mass concentration of 1 mm of water spread over a circular area of 400 km diameter (130 million tons) is shown at right in Figure 1. The peak in the signal power for such a mass distribution is around 4 mHz, where the improved tidal acceleration metrology is roughly 60 times improved over GRACE-FO with a 1 pm/s^2/Hz$^{1/2}$ TM, with the integrated SNR for a single pass over such a gravitational perturbation from roughly 0.5 to 30.

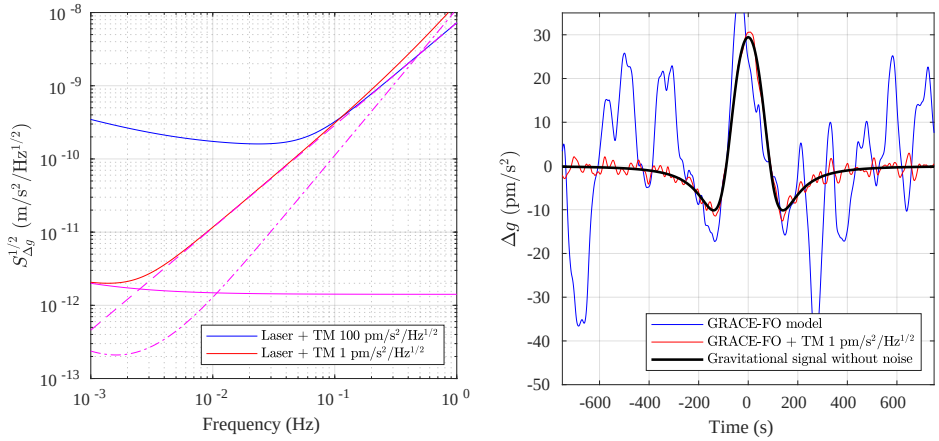

Figure 1. (**Left**) Differential acceleration sensitivity of a two SC geodesy measurement, considering simplified models for GRACE-FO laser frequency and TM acceleration noise (blue) and, in red, the expected performance with GRACE-FO interferometry coupled with the improved GRS TM system studied here, including noise in the GRS TM acceleration and readout. Contributions of TM stray accelerations (solid), laser frequency noise (dashed), and the local TM readout (dash-dot) are shown in magenta. Some drag-compensation is assumed both in order to achieve the acceleration noise requirement and to limit stiffness coupling to GRS readout noise, both relevant only near the 1 mHz lower frequency limit (this includes applied TM forces in the ± 50 pm/s^2 range, with associated stiffness $\omega_{xx}^2 \approx 1.25 \times 10^{-4}$/s^2). (**Right**) Simplified simulated differential acceleration signal and noise from a "mascon" with a 1 mm layer of water spread over a 400 km diameter circle in the two configurations (for visualization a 4th order low pass filter with 15 mHz corner frequency is applied to signal and noise in both cases).

We note that this signal time scale of roughly 250 s, 20 cycles per orbit, and corresponding 4 mHz peak in signal power is roughly unchanged for smaller mass anomalies; mass distributions of several hundred kilometers are already approaching the "point-mass" limit with a 500 km orbital height. Improving TM acceleration noise thus improves sensitivity at all "useful" geodesy frequencies, dramatically in the 1–10 mHz band that is the natural range set by low Earth orbits in a GRACE-like mission.

This differential acceleration measurement noise is not the only relevant source of uncertainty in extracting a model of the Earth's gravity or mass distribution; a two spacecraft mission sampling a given point on the Earth at roughly two week intervals "undersamples" the gravitational changes caused by weather; local mm-scale water equivalent height mass anomalies can be overwhelmed by local variations in the roughly 10 m equivalent H_2O height of the atmosphere mass, introducing a significant aliasing effect. This problem can be addressed by multiple satellite pairs in appropriately coordinated orbits, which will be introduced in the ESA—NASA NGGM mission [11] and perhaps other future inter-agency projects.

Considering these possibilities to address the aliasing problem with a growing constellation of intersatellite geodesy pairs, reducing the noise from TM acceleration can facilitate a substantial scientific gain in the measurement and modeling of terrestrial gravitational changes.

Top Geodesy GRS Design Requirements

We take as a reference stray TM acceleration noise level

$$S_g < \left(1\,\mathrm{pm/s^2/Hz^{1/2}}\right)^2 \tag{2}$$

in the 1–100 mHz band. The $\mathrm{pm/s^2}$ has been motivated and requested in various studies [8,10], and allows the mission to take advantage of the current laser-frequency noise floor nearly across this entire frequency band. It also coincides with a performance where other factors, like pointing and spacecraft orbit determination become relevant [10]. Although various known noise sources will increase going to lower frequencies, we include no "relaxation" in this design goal; meeting this performance around 1 mHz, where the TM will rival interferometry noise in limiting mission performance in our simplified model (see Figure 1), will depend on key mission parameters as discussed shortly.

We take as a reference noise limit for the GRS position sensing at the level

$$S_{x_{TM}} < \left(200\,\mathrm{pm/Hz^{1/2}}\right)^2 \times \left[1 + \left(\frac{5\,\mathrm{mHz}}{f}\right)^2\right] \tag{3}$$

Referring to the final term in Equation (1), we see $S_{x_{TM}}$ is relevant both as an effective measurement noise, at higher frequencies, and for the "stiffness" coupling to SC motion at low frequencies. We set the "white noise" floor at 200 $\mathrm{pm/Hz^{1/2}}$ to be well below the noise floor set by the laser—in terms of the "one way" link displacement noise, at 100 mHz we have $2S_{x_{TM}}^{1/2} \approx 400\ \mathrm{pm/Hz^{1/2}}$ against roughly $\sqrt{2}LS_{\Delta\nu/\nu}^{1/2} \approx 1\ \mathrm{nm/Hz^{1/2}}$ from laser frequency noise. At 1 mHz, we would try to keep TM displacement sensing noise below 1 $\mathrm{nm/Hz^{1/2}}$. We will see that the stiffness coupling, at least in a worst case "full accelerometer" configuration, can be important, with $\left|\omega_{xx}^2\right| > (2\pi \times 1\,\mathrm{mHz})^2$.

Among the other performance requirements, the electrostatic actuation force authority—known as the "measurement range" for an accelerometer—is a key parameter impacting design and performance. Accelerometry data from GRACE-FO shows a typical along-track SC drag acceleration of roughly 300 $\mu\mathrm{m/s^2}$ [12], with large orbital "day-night" peak–peak variations up to many tens of $\mathrm{nm/s^2}$ and longer term variability with the solar cycle. Missions reaching down to 400 km altitude expect drag accelerations up to roughly $\mu\mathrm{m/s^2}$ [11]. We consider as a reference electrostatic actuation authority requirement of 1 $\mu\mathrm{m/s^2}$, with comments on the impact of varying this.

3. Key Design Elements and Performance Characteristics for Geodesy GRS

The top level geodesy performance drivers of Equations (2) and (3) are compared with the analogous requirements for the LISA GRS: 3 fm/s^2/Hz$^{1/2}$ TM acceleration noise and 1.8 nm/Hz$^{1/2}$ capacitive sensing displacement noise. The extreme limits on TM acceleration noise, five orders of magnitude below the "state of the art" for what was the "future" GRACE mission at the time of the LPF design around 2000, drove the choice of a large, heavy TM—a Au-Pt cube with $s = 46$ mm and $M = 1.93$ kg—and large TM-EH gaps—4 mm on the critical x axis. This addressed a variety of surface force noise sources, mainly, but not exclusively, electrostatic, for which there was limited experimental data and which the force amplitude increases with decreasing TM-EH gap—as d^{-1} for stray DC potentials and cosmic ray charge noise, as d^{-2} for electrode voltage noise interacting with stray DC potentials and for Brownian gas damping noise, as d^{-3} for force gradients from stray DC potentials. The resulting accelerations all decrease with TM mass, $M = \rho s^3$, in spite of their increase with surface area s^2. The LPF GRS, designed both for testing with LPF and use in the LISA gravitational wave observatory, thus chose the largest and heaviest TM, with the largest possible gap, that was still compatible with both "launchability"—for overall system mass and the ability to hold the TM during launch vibrations—and with still achieving the modest 1.8 nm/s^2 capacitive sensing noise requirements, whose sensitivity improves with smaller gap [4,5,13].

Moving to a heavier, more isolated TM in a more spacious electrode housing conducting shield introduced design complications that were essential for a LISA GRS but not warranted in early satellite geodesy missions. The larger TM-EH gaps limit capacitive position sensitivity, requiring use of a "local" TM interferometer [14] to reach the 10 pm/s^2 position sensitivity needed along the critical gravitational wave x science axis, with 1.8 nm/Hz$^{1/2}$ sufficient for spacecraft control on the non-science axes. The larger TM with a multi-mm course of motion requires a launch lock and release mechanism system not present in geodesy accelerometers [15,16]. Reducing force noise from stray electrostatics required development of AC-drive (audio frequency carrier) electrostatic suspensions [4]. The removal of the discharge wire to eliminate a dominant source of mechanical force noise requires adding a UV discharge system to maintain TM neutrality against cosmic ray charging with a truly "floating" TM [17].

We use the LISA Pathfinder heritage design as a starting point, aiming to simplify and lighten the GRS system where possible. A move to smaller gaps is both allowed by the relaxation from fm/s^2 to pm/s^2 and dictated by the desire to improve capacitive position sensing by roughly a factor 10, to avoid having to introduce an interferometric TM readout. Moving to the smallest TM still compatible with the acceleration and sensing noise requirements will limit overall system mass and, combined with smaller TM-EH gaps, allow simplification of the TM launch lock and release mechanism system. We will consider designs with mass below 1 kg and gaps not exceeding 1 mm.

3.1. Strawman GRS Design

We assume a cubic TM made from Au-Pt as in LISA, chosen for its high density and magnetic purity. The TM-EH system has the same electrode configuration—functionality and number—as the LISA design, a 6DOF gap-sensing design with two sensing electrodes (green in Figure 2) on each of the six cubic faces. The x axis is considered as the privileged axis defined by the inter-spacecraft axis for the geodesy science measurement. Additional "injection electrodes" (red in Figure 2) are placed on the Y and Z EH faces to provide a contact-free TM AC bias voltage for the TM capacitive position readout; including them on the X face as well would limit the critical x axis sensing and introduce important electrostatic stiffness.

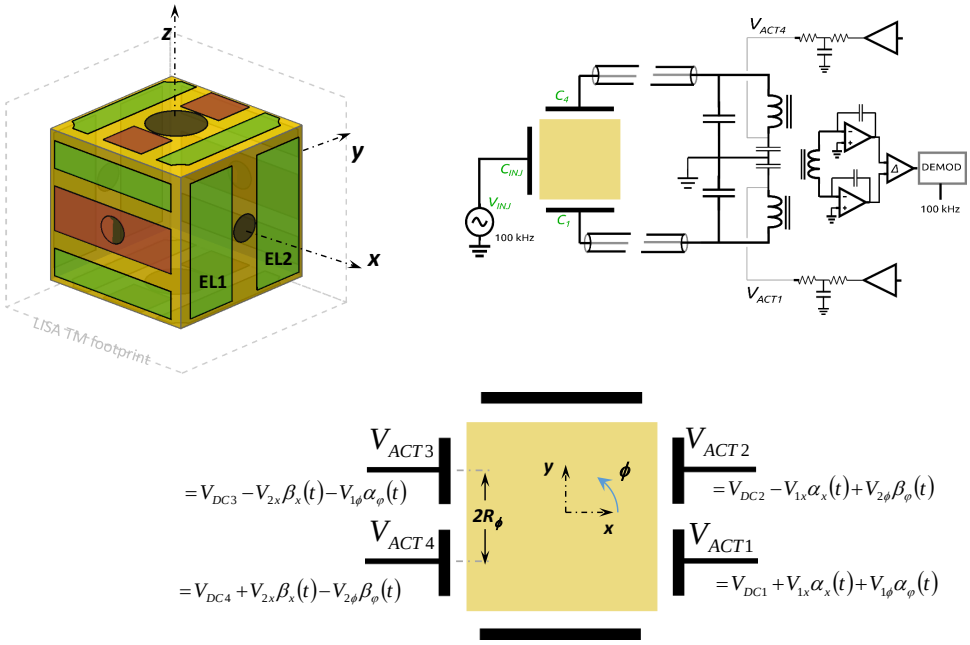

Figure 2. Sketch of strawman electrode housing and TM, with associated sensing and actuation electronics at upper right and, lower right, *X* face electrode actuation configuration for x forces and ϕ torques.

The *Z* faces also provide access holes for mechanisms to cage and release the TM. We assume the same EH interface features to accommodate this: an enlarged "plunger" access hole on the center of both *Z* faces (12 mm diameter), for low-force ($\sim$ 1 N) in-orbit TM grabbing and positioning [16,18] and space for four caging launch lock "fingers" ($\sim$ 1.2 kN) mating to spherical features on the corners of the TM [15], removing quarter-circles of roughly 3 mm radius from the "useful" surface of the *Z* electrodes. We take the LISA mechanisms access as a conservative approach, considering possible reductions due to the smaller TM for geodesy.

On the *X* and *Y* faces we include here 6 mm holes from the LISA design. Their possible inclusion will have to be studied for possible laser beam access—their original purpose, at least for *X*—but also molecular conductances and inspection purposes during integration.

The TM and EH, with accompanying mechanisms, will be mounted in and enclosed by a dedicated vacuum chamber vented to space through a vent duct, with the LPF heritage solution coupling the vent valve and launch lock in a single one-shot "caging venting mechanism" [15]. The vacuum chamber will also contain mounting points for gravitational balance masses, which in the LPF heritage were used to bias the gravitational field at the TM with up to 25 nm/s^2 "authority" along the x axis with a 2 kg tungsten mass inside the vacuum chamber. Additional gross balancing and fine tuning is possible from mounting points outside the chamber, with sub-nm/s^2 precision designed and achieved in LPF [2,19].

The vacuum chamber will also include fiber injectors for UV illumination of TM and EH surfaces, used for photoelectric discharge of the TM. The discharge concept has been demonstrated with Hg lamp light sources in LPF [20], with an improved system based on UV LEDs under development for LISA [21]. The exact positioning and number of needed illumination ports remains to be defined, but some form of discharge should be included in the geodesy GRS.

We assume electronics heritage from the LPF design, which has been led by ETH Zurich [22–24]. Capacitive position sensing is provided by a resonant capacitive-inductive bridge, sketched at right in Figure 2 [4,22], relying on a highly balanced differential transformer ($\frac{\Delta L}{L} < 50$ ppm) for intrinsically high common-mode rejection in the comparison of AC currents flowing from the TM into pairs of opposing sensing electrodes. An excitation frequency near 100 kHz is chosen, with parasitic capacitance tuned for *LC* resonance to

optimize impedances for the differential trans-impedance amplifiers, which allow a simple differential current readout and hold the electrodes and their >1 m coaxial lines at virtual ground, reducing parasitic capacitance errors. Such bridges, one for each of the 6 sensing channels—2 channels are combined to give translational and rotational displacements—have been demonstrated in LPF, yielding aF/Hz$^{1/2}$ sensitivity for a 0.6 V TM AC bias [23], near the thermal noise limit of the transformers.

The LISA electrostatic actuation force and torque actuation system based on AC carrier voltages would be well suited for the geodesy GRS. The quadratic relation of force to applied voltage, $F \propto V^2$, allows DC or slowly varying control forces with audio frequency—above the science band—AC carriers, avoiding coupling to DC potentials from TM charge and patch voltages. Opportune zero-mean, orthogonal waveforms—for the x/ϕ DOF referred to generically as $\{\alpha_x, \beta_x, \alpha_\phi, \beta_\phi\}$ (see Figure 2) effectively decouple the different DOF. Additionally, we hold constant the sum of the squared voltages, for instance $\left(V_{1x}^2 + V_{2x}^2\right)$ and $\left(V_{1\phi}^2 + V_{2\phi}^2\right)$, in order to maintain the actuation force gradient "stiffness" constant and to limit force-torque cross-coupling for an off-center TM. This constant stiffness audio carrier actuation architecture was recognized as necessary early in the LISA Pathfinder development [4] and was implemented in LPF using α and β sine/cosine waveforms at different frequencies for the 6 actuation DOF [24].

Although LPF had two sensing/actuation modes with a range switch—between a low force/high position sensitivity science mode and a higher force, wide sensing range acquisition mode—it is possible that a single range might cover the geodesy needs, and we comment on the corresponding implications in the following subsections.

The designs of the TM/EH geometry and sensing/actuation electronics are tightly coupled in any evaluation of performance and functionality. Although the following performance discussion is parametric, at least in the TM side length (s)—and resulting mass M—and TM-EH gap (d), and based mostly on simple scaling, we take as a starting point $s = 34$ mm ($M \approx 790$ gm for Au-Pt), with symmetric gaps of $d_x = d_y = d_z = 800\ \mu$m, illustrated in Figure 2. Fitting the electrodes, including guard ring surfaces, as performed for LPF [4] results in a design as in Figure 2, with key parameters summarized in Table 1, with some flexibility in optimizing the ratio of injection to sensing surfaces, based on more detailed requirements for the performance requirements on different axes.

Table 1. Comparison of "strawman" geodesy GRS considered here with the LPF GRS design, for key TM/EH/electronics design parameters.

		LISA	**GEO GRS Strawman**	
cube sidelength	s	46 mm	34 mm	
TM mass	M	1.93 kg	790 g	Au-Pt
TM-EH gap	d	4/2.9/3.5 mm	800 µm	
sensing electrodes		2 sensing EL per face		gap sensing
injection electrodes		Y, Z faces		split on Z
total TM capacitance	C_{TOT}	$\approx$ 35 pF	$\approx$ 80 pF	
X capacitance	C_X, $\frac{\partial C_X}{\partial x}$	$\approx$ 1.2 pF, 0.3 pF/mm	$\approx$ 4 pF, 5 pF/mm	
100 kHz TM bias	V_{TM}	0.6 V	0.3 V	
max AC act voltage	V_{MAX}	$\pm$10 V/$\pm$135 V	50 V	double/single range

The logic of this starting point and criteria for fine tuning are presented in the following subsections, which address key performance drivers depending strongly on the choices of s and d, each of which plays a significant role in the LISA GRS heritage and overall performance: capacitive sensing and electrostatic actuation—each from the standpoints of functionality, noise performance and electrostatic stiffness—and residual gas damping. The range of TM mass and gap size will also define the design space for the critical system of mechanisms for TM launch lock and release. Some comments are given at the end on remaining noise sources mainly related to the environment and its orbital dependence.

This simplified analysis of key performance drivers is just a starting point, and a more detailed trade-off will be proposed to study a full implementation based on additional engineering considerations. This will include an iteration for mechanisms accommodation and design, and requirements on dimensional and alignment tolerances, which will likely be a more stringent driver with the smaller TM-EH gaps. Finally, it will also include a deeper analysis of the detailed dynamic control, regarding the different use cases for the GRS as a position sensor and force actuator in various possible mission scenarios.

3.2. Capacitive Position Sensing

Considering a differential capacitance readout with effective capacitance noise, $S_{\Delta C}$, the resulting displacement measurement noise can be determined by the capacitance derivative for the given sensing electrode, $\frac{\partial C_X}{\partial x}$ in this case, and combining two adjacent sensing channels:

$$S_x \approx \frac{1}{2} \frac{S_{\Delta C}}{4\left|\frac{\partial C_X}{\partial x}\right|^2} \propto S_{\Delta C} \left(\frac{d}{s}\right)^4 \tag{4}$$

The capacitance sensitivity $\frac{\partial C_X}{\partial x}$ scales with electrode surface—proportional to s^2—divided by the gap squared, d_x^2. For a 34 mm cube and the 1 aF/Hz$^{1/2}$ noise demonstrated in LPF at TM AC bias $V_{TM} \approx 0.6$ V, the required 200 pm/Hz$^{1/2}$ is reached for gaps below roughly 1.25 mm (see upper left of Figure 3). At $d_x \approx 800$ µm, the needed position sensing is achieved, with some margin (140 pm/Hz$^{1/2}$) with half the TM 100 kHz bias (0.3 V amplitude) and, thus, relaxed capacitive noise requirements (2 aF/Hz$^{1/2}$).

Meeting the sensing requirement (Equation (3)) with larger gaps could in principle be managed by increasing sensitivity with an increased V_{TM}, at least for the "additive" sources, such as from the transformer thermal noise and by the trans-impedance amplifier voltage and current noise. For additive noise sources, $S_{\Delta C} = \frac{S_{\Delta C}^{NORM}}{V_{TM}^2}$, where $S_{\Delta C}^{NORM}$ is independent of the TM bias voltage V_{TM}. For the dominant transformer thermal noise in the LPF electronics, this is $S_{\Delta C}^{NORM} \approx \frac{8k_BT}{\omega_0^3 LQ} \approx \left(0.45\text{V aF/Hz}^{1/2}\right)^2$, where L and Q are the transformer primary inductance and quality factor and $\omega_0 = 2\pi \times 100$ kHz [23]. Although improvement into the sub-aF/Hz$^{1/2}$ range with increased V_{TM} is probable, it will be limited at some level by parasitic capacitance or interference pickup. We thus conservatively rely here on a relaxed LPF heritage performance, actually relaxed here by a factor two.

Considering the total injection capacitance, roughly 8 pF, we will need to apply an injection voltage of roughly $V_{INJ} \approx 3$ V amplitude to obtain the 0.3 V TM bias, with $V_{TM} = V_{INJ}\frac{C_{INJ}}{C_{TOT}}$ (ratio of TM capacitance to the injection electrode and the total TM capacitance to the electrode housing).

The corresponding rotational ϕ sensitivity is roughly that of Equation (4) divided by R_ϕ, half the on-center separation between the two X electrodes (9.5 mm in the strawman design in Figure 2), giving roughly 15 nrad/Hz^{Hz}. Due to the presence of injection electrodes on the Y and Z EH faces and consequent reduction in sensing surface area, the displacement sensing noise on the associated y/θ and z/η DOF will be worse, roughly 300 pm/Hz$^{1/2}$ and 25 nrad/Hz$^{1/2}$.

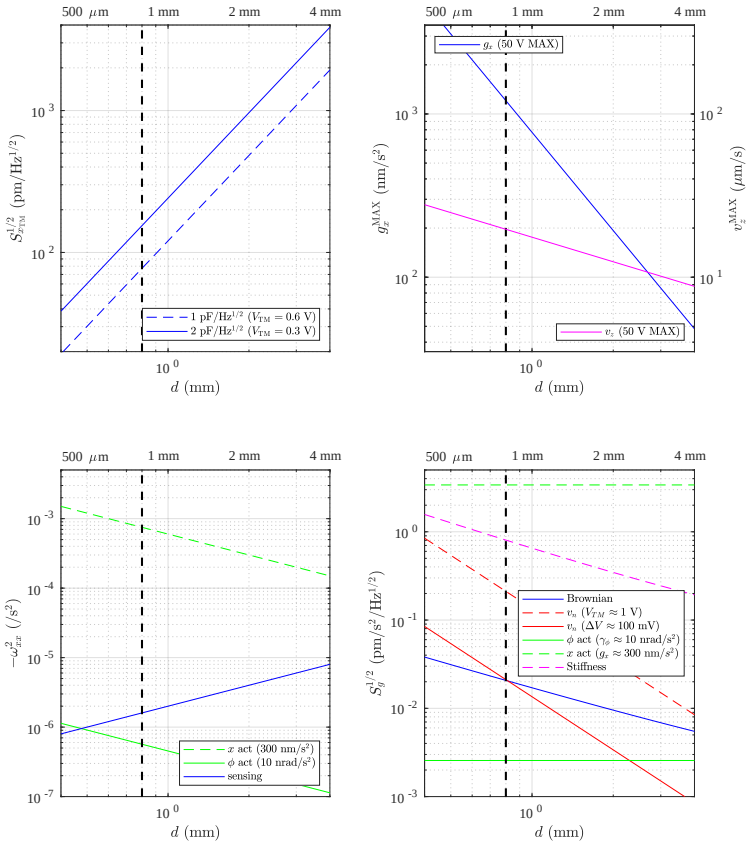

Figure 3. Key performance parameters for the studied GRS design as a function of the TM-EH gap d, assuming a cubic TM of side length $s = 34$ mm (reference design gap of 800 μm is indicated with a vertical dashed black line). (**Top left**) Displacement sensing "white noise" performance for fixed levels of capacitive sensing noise $S_{\Delta C}$. (**Top right**) Maximum x actuation force and maximum allowed TM z velocity allowing to stop the TM at no more than half the sensor Z gap. (**Bottom left**) Main sources of force gradient or "stiffness". (**Bottom right**) Simple scaling of several known key TM acceleration noise sources evaluated at 1 mHz.

Assuming the same LPF bridge saturation limit, we would have roughly ±25 μm full scale motion of the TM along x and nearly double this on y and z. Though likely sufficient for science operations, this range would likely need to be extended—to perhaps half the gap—for initial acquisition and TM release operations where larger displacements can be expected. This does not require a range switch but can be achieved by decreasing the 100 kHz injection voltage, by a factor 20—to 150 mV—to guarantee coverage over at least half the "wall-to-wall" TM motion, either by a digital amplitude setting or a single switched step-down transformer stage at the GRS injection generation.

We finally note that the suggested low frequency relaxation in Equation (3), to 1 nm/Hz$^{1/2}$ at 1 mHz, allows some margin for low frequency effects observed in LPF, both gain dependent and additive [23], but this does not look overly demanding.

Sensing Stiffness

The TM bias creates an x axis electrostatic force gradient quadratic in the V_{TM}, described by a negative stiffness

$$\omega_{xx}^2 \approx -\frac{1}{2M}\frac{\partial^2 C_{TOT}}{\partial x^2}\frac{V_{TM^2}}{2} \propto \frac{V_{TM}^2}{sd^3} \propto \frac{d}{s^5}\frac{S_{\Delta C}^{NORM}}{S_{x_{TM}}} \quad (5)$$

In the last expression, used in Figure 3 (lower left) we assume sensitivity scaling with V_{TM}, illustrating the stiffness cost associated with trying to obtain low noise position sensing with a much smaller TM.

Our reference design gives a sensing stiffness of roughly 1.6×10^{-6} /s^2 on the sensitive x axis. This is a small fraction of the electrostatic stiffness caused by actuation in an accelerometer usage (see next section), but is larger than the entire LPF measured stiffness of roughly 0.5×10^{-6} /s^2 [25] and, in a drag-free mission might indeed become the dominant source of force gradient coupling to the spacecraft. Although the LISA/LPF stiffness is mainly gravitational [25], the geodesy GRS will likely be dominated by electrostatics, even without considering actuation, given the smaller test mass and gaps. Stiffness grows to roughly 10×10^{-6} /s^2 on y and z, where the injection fields count directly.

3.3. Electrostatic Force Actuation

For electrostatic actuation, we consider audio frequency sinusoids applied to each electrode for both force and torque, with the same symmetry shown at lower right in Figure 2, at 6 different audio frequencies for the 6 DOF, and using the constant stiffness actuation algorithm mentioned above. We consider a total maximum instantaneous peak voltage V_{MAX}, initially allocated in equal parts $\frac{V_{MAX}}{2}$ to force and torque. Considering the time averaged (in-band) actuation force $F \propto \langle V^{MAX} \rangle$, we will have a maximum mean square voltage for TM translational acceleration of $\frac{V_{MAX}^2}{8}$. This is conservative, as it is likely that the control torques will allow a larger fraction of the available voltage for force, with an in-flight adjustment allowing to increase the maximum force by up to a factor 4 in the limit of vanishing torques. It is also sub-optimum from the standpoint of maximum force per voltage, compared for instance to DC voltages which give a factor two increase in the mean square voltages. However, this "science" scheme could possibly be used for all actuation conditions, including possible accelerometer use and TM release in a geodesy sensor, so we consider this here.

The maximum x axis actuation authority is

$$g_{MAX} \approx \frac{1}{M} \left| \frac{\partial C_X}{\partial x} \right| \frac{V_{MAX}^2}{8} \propto \frac{1}{sd^2} V_{MAX}^2 \tag{6}$$

and is illustrated at top right in Figure 3. At 800 μm gap a ±50 V voltage range allows authority slightly more than 1 μm/s^2 (roughly 60 nrad/s^2 in ϕ torque, with the possibility to increase force, by up to a factor 4, at the expense of the torques). The y and z axis forces are slightly lower for the reduced electrode surface area. The LPF GRS, with heavier TM and larger gaps, provided lower TM accelerations, up to roughly 0.5 μm/s^2 with a larger maximum voltage of 135 V.

The maximum forces are key for possible accelerometer operation in a science mode without any SC drag compensation but also for TM control following release. We can give a rough estimate of the maximum controllable release velocity along the most critical TM z axis of the release system, using conservation of momentum, equating the change in the capacitive energy, $\frac{1}{2}\langle V^2 \rangle \Delta(C)$ summed over the two "pulling electrodes", with the change in kinetic energy, $\frac{M}{2}\left(v_z^{MAX}\right)^2$. Considering as a maximum allowable TM excursion of $\frac{d_z}{2}$—thus $\Delta C_z \approx \frac{C_z}{3}$—we obtain

$$v_z^{MAX} \approx \left(\frac{C_z V_{MAX}^2}{12M} \right)^{1/2} \propto \frac{V_{MAX}}{(sd_z)^{1/2}} \tag{7}$$

Again, there is an improvement in going with smaller gaps and a lighter TM, and the reference design considered allows to stop TM with velocities slightly beyond 20 μm/s. This is slightly optimistic, neglecting controller response time to the moving TM (the theoretical stopping times for this maximum allowed velocity are of order 20 s) and multi-DOF dynamics. The LPF TM release system was designed for 5 μm/s release velocities,

but observed values were often outside this range [18]. The system is under review and optimization for LISA, and, while the smaller geodesy mass and gaps should simplify the system, the LISA development will be useful also for the geodesy TM release.

If the $\mu m/s^2$ actuation forces allowed in this design by a ± 50 V AC range are indeed sufficient for the geodesy applications, the simplification to a single range electronics is worth considering. Considering the 17-bit resolution of the LPF electronics—roughly 150 μV in a ± 10 V AC science range [24]—and expanding this to a ± 50 V range, the amplitude LSB would also increase by a factor 5 to 750 μV. For use in science acquisition without any drag-free compensation, electrostatic compensation of $g_c \approx 300$ nm/s^2 would require roughly 10 V amplitude applied voltages. The relevant "acceleration LSB" is roughly $2g_c \frac{\Delta V}{V} \approx 50$ pm/s^2. This appears large compared to the pm/s^2/Hz$^{1/2}$ level and requires more detailed control analysis, but in extracting the "external" gravitational accelerations, such as for geodesy (see Appendix A) or LPF [2,24,25], the critical performance driver is not the resolution of the actuator quantization but rather the accuracy with which the actuator force is calculated. If necessary for the controller, a high frequency "dithering" of the force command could also be used in a $\Sigma - \Delta$ controller, if necessary, to effectively average to a higher resolution. Using a single actuation/sensing range would be a simplification with respect to the LPF electronics, which required switching both on sensing and actuation channels.

3.3.1. Actuation Gain Fluctuations and Force Noise

We can consider every actuating electrode k, contributing g_k to the TM force per unit mass, with a fluctuating actuator gain factor, $\frac{\Delta V_k}{V_k}$, as introducing an acceleration fluctuation $\delta g \approx 2g_k \frac{\Delta V_k}{V}$. In LISA Pathfinder, in preparations on the ground [26] and then in-flight [3], it was observed that the dominant fluctuations were uncorrelated between the electrodes, at levels $S^{1/2}_{\Delta V/V}$ between 3 and 8 ppm/Hz$^{1/2}$ at 1 mHz across the different actuator amplifiers [26], rather than coming from voltage references or other "common mode" gain fluctuations. Considering the effect of two incoherently fluctuating actuators, each pulling half the actuator load in x, the acceleration noise is

$$S_g^{ACT} \approx 2\, g_c^2\, S_{\Delta V/V} \tag{8}$$

This is independent of the EH/TM dimensions. Assuming the worst case performance of 8 ppm/Hz$^{1/2}$ at 1 mHz, we would have, in the case of 300 nm/s^2 actuation forces, roughly 3 pm/s^2/Hz$^{1/2}$, thus alone breaking the total pm/s^2/Hz$^{1/2}$ TM acceleration noise budget (see bottom right plot in Figure 3). This scales with the applied forces, so even a partial reduction of the actuation load could bring noise below the pm/s^2/Hz$^{1/2}$ level. Similar improvements could be possible in the actuation electronic stability but require study.

In a truly drag-free system, x axis forces would not be needed and the situation dramatically changes. ϕ rotational actuation would always be needed to keep the TM aligned to the SC, which needs to point to the distant SC to align the intersatellite optical measurement. Certainly any DC torque from SC "self-gravity" would require DC compensation, and any orbitally varying pointing manuevers, needed to correct orbits or other, would introduce additional torque actuation. Self-gravity torques on the TM are mostly coming from very close to the TM—the torque on a cube from a point mass at a distance r decreases as r^{-5}—and mostly inside the GRS. LPF showed the ability to control the DC angular accelerations to better than 1 nrad/s^2 [3,19]. If we assume actuation torques up to 10 nrad/s^2 and the same uncorrelated actuation gain noise as above, we will have roughly 3 fm/s^2/Hz$^{1/2}$ at 1 mHz, thus a contribution orders of magnitude below the total allowed noise.

We note that x acceleration noise from ϕ actuation can be eliminated by moving ϕ actuation—and sensing—to electrodes on the Y faces of the GRS, such that there are no noisy fields on the TM x axis introduced by ϕ electrostatic torques. The resulting design would have a single large X electrode and 4 smaller electrodes dedicated to $y/\theta/\phi$ DOF

on the sensor Y faces. Such a design was considered for LISA Pathfinder [4] and recently for geodesy, in Ref. [10]. This single-X electrode configuration also reduces, by a factor 2 in power, the sensing noise while increasing the force noise from x actuation by a factor 2 and slightly reducing the envelope for $y/\theta/\phi$ actuation. It could slightly complicate machining and integration, with more parts, and introduces some asymmetry between sensing/actuation channels. At least for the ϕ torques and sensing performance considered here, deviating from the LISA design with 2 sensing/actuation electrodes per X face does not seem necessary but could be studied.

3.3.2. Actuation Stiffness

The x axis actuation stiffness is related simply to maximum applied forces and gap:

$$\omega^2_{xx(\mathrm{ACTx})} \approx -2\,\frac{g_c^{MAX}}{d_x} \tag{9}$$

For use with a 300 nm/s^2 range, we will have roughly -750×10^{-6}/s^2 stiffness. This dominates all other stiffness sources (see bottom left in Figure 3) but also inertia itself in the mHz regime, with $\frac{|\omega^2_{xx}|^{1/2}}{2\pi} \approx 4.4$ mHz. Considering 1 nm/Hz$^{1/2}$ sensing noise at 1 mHz in the stiffness correction, we would have 0.75 pm/s^2/Hz$^{1/2}$ from this noise source, not quite at the level caused by actuation gain fluctuations but not far off.

The x axis actuation stiffness from ϕ torques would be a small factor at 10 nrad/s^2 actuation torques, behind sensing stiffness.

3.3.3. In-Band Actuation Voltage Noise and Low Frequency Electrostatics

"In-band" additive actuation voltage noise mixes with any stray DC potential differences—from patch potentials and TM charge [27–31] —to cause low frequency force noise. We can describe this by a change in force from one electrode by $\Delta F \approx \frac{\partial C_X}{\partial x}\,\Delta V_{DC}\,v_n$, where ΔV is some stable DC potential difference between electrode and TM, and v_n is some electrode actuation voltage fluctuation. Summing over 4 X electrodes, we obtain

$$S_g^{v_n} \approx \frac{4}{M^2}\left|\frac{\partial C_X}{\partial x}\right|^2 (\Delta V_{DC})^2 S_{v_n} \propto \frac{1}{s^2 d^4}(\Delta V_{DC})^2 S_{v_n} \tag{10}$$

LPF acceleration noise measurements with a charged TM [27] allowed resolution of the electrode voltage fluctuations, at roughly the 20 μV/Hz$^{1/2}$ at 1 mHz. In the simplest implementation of increasing the science mode voltage range by a factor 5 with an amplifier, we could have a worst case increase of a factor 5 in this low frequency voltage noise (an alternative with a step-up transformer only for increasing the audio frequency amplitudes should leave the low frequency noise unchanged but might add complexity). We consider also a conservative value of 100 mV DC potential difference, which could be a reasonable discharge threshold but also not much worse that typical electrode stray potentials. This results in roughly 0.1 pm/s^2/Hz$^{1/2}$ acceleration noise, not threatening to the pm/s^2/Hz$^{1/2}$ goal.

It is worth mentioning that, at least with this level of actuation voltage noise, the choice of audio frequency carriers for force actuation would seem well justified. In the case of a "DC drive" actuation, we would need roughly 7 V DC voltages, which becomes the V_{DC} in Equation (10) (with a factor 2 instead of 4, for the dominant DC actuation voltage on 2 relevant pulling electrodes). This would give roughly 4 pm/s^2/Hz$^{1/2}$, thus a leading noise source along with the actuation gain fluctuations. Additionally, the stray DC biases of order 100 mV would induce changes in the applied actuation force of order 10 nm/s^2. Moving to audio frequency voltages thus removes both relevant force noise and inaccuracy.

3.4. Brownian Motion from Residual Gas Damping

Brownian noise from gas damping was also "discovered" to depend on the TM-EH separation in preparation for LPF [32], with the closely spaced surfaces introducing significant correlations between successive impacts of the same molecules. This was the limiting source of noise in LISA Pathfinder at mHz frequencies [3]. The scaling of this noise source is

$$S_g^{Br} \propto \frac{1}{M^2} p s^2 \frac{s^2}{d^2 \ln \frac{s}{d}} \propto p \frac{1}{s^2 d^2 \ln \frac{s}{d}} \tag{11}$$

LISA Pathfinder obtained 1 μPa pressure by the end of mission [3], using a vent-to-space system through a short (25 cm) tube with roughly 10 cm^2 section (15 l/s pumping impedance). The external pressure in a GRACE-like orbit should offer sufficiently low atmospheric pressure to allow such performance [33], but we lack details on the integration of such a conduit to space in a realistic geodesy spacecraft. Assuming a 10 μPa pressure inside the geodesy GRS, this noise source will be around 20 $fm/s^2/Hz^{1/2}$, well below the requirements, though integration and interaction with the variable atmosphere need to be understood.

3.5. Other Key Force Noise Sources

Several other noise sources are much more dependent on the spacecraft and orbital environment than on the TM/EH dimensional configurations and sensing/actuation electronics, most prominently thermal and magnetic couplings. These are perhaps best considered as systematic error signals in competition with the Earth position-dependent gravitational "science signal", both driven by quasi-periodic orbital modulations and, thus, a dependence, or apparent dependence, on Earth position and solar exposure via the orbit. The forcing—order degrees K and Gauss variations—is orders of magnitude beyond observed field and temperature excursions in LPF [34,35], with harmonics of the roughly 0.2 mHz orbital modulations leaking into the relevant mHz band. The couplings are well understood—coefficients $\frac{\partial g}{\partial T}$ and $\frac{\partial g}{\partial \Delta T}$ coupling to fluctuations in mean GRS temperature and temperature gradient [3,36], and the magnetic field gradients near the TM [34]—and mitigation is possible. The temperature driven forces can, if necessary, be measured in dedicated heating experiments and subtracted based on thermometer readouts, while, as found in Ref. [10], magnetic shielding can attenuate the relevant fields.

Additional systematic orbital modulation should be studied as well for TM charging, residual atmosphere reentry into the GRS via the vent duct, and thermoelastically-driven gravitational forces from the spacecraft.

4. Conclusions

Removing the discharge wire, increasing TM mass and widening the gaps between TM to surrounding electrode housing surfaces, can limit the spurious accelerations from surface force noise effects well below the $pm/s^2/Hz^{1/2}$ level that is desired for geodesy science. This has been shown experimentally with the LISA Pathfinder GRS, with three orders of magnitude margin, and our analysis indicates that a smaller and simpler GRS system is compatible with the target levels. Additionally, testing GRS surface force noise on ground, to the required $pm/s^2/Hz^{1/2}$ level, is possible with torsion pendulum experiments directly sensitive to force on the relevant TM x axis [37,38]. Although the conclusions reached here are fruit of a simple analysis, they can be verified and "de-risked" on ground before launch.

Our simplified analysis of a strawman GRS design also indicates that the GRS capacitive readout can be sufficiently precise, 200 $pm/Hz^{1/2}$, to take advantage of the inter-spacecraft interferometry measurement without the additional complication of extra interferometric TM readouts.

The remaining challenges to improve on the TM acceleration noise in low-Earth orbit are mainly environmental, associated with systematic force effects from orbitally modulated disturbances and, in particular, noise associated with electrostatic actuation forces when

using the TM in an accelerometer configuration without any thrust compensation of SC drag. Our rough analysis indicates that reaching $\mathrm{pm/s^2/Hz^{1/2}}$ with 300 $\mathrm{nm/s^2}$ TM forces would be difficult, perhaps violating by a factor of roughly 3 with the LPF actuation performance. Force gradient stiffness, again set by the level of actuation forces, and the resulting coupling to the spacecraft motion, would be only slightly smaller (see bottom right of Figure 3). This slightly degraded performance would already be a big improvement in geodesy performance, relevant across the entire useful band. However, even a partial compensation of the SC drag with thrusting—even a static, open-loop thrusting that reduces the required electrostatic forcing to the level of "day–night" modulation, with 10s of $\mathrm{nm/s^2}$ peak values, would bring the overall TM acceleration noise below $\mathrm{pm/s^2/Hz^{1/2}}$.

The strawman GRS design presented here is just a starting point for a more complete implementation of a geodesy GRS. The simple scaling of relevant parameters indicates that there is margin for going smaller than the 34 mm, 790 g Au-Pt cube considered in this exercise. Part of a detailed study of implementing a full GRS for geodesy should be to understand if further reductions in M can be implemented reliably and with an appreciable impact on lowering system mass and complexity.

Finally, the TM performance in LISA and LISA Pathfinder benefits from a system "built around" the GRS, giving a stable and isolated thermal, electromagnetic, gravitational, and dynamic control environment around the TM. This is an obvious design strategy, as TM acceleration noise is the limiting factor for most of the observatory science. Given the essential role of the geodesic reference mass in the science return of a GRACE-like mission, a similar approach is worthwhile in integrating a GRS into future geodesy mission. Although opportunities to "add on" a GRS sensor as a technology demonstrator might offer the quickest possibility to put such a system in orbit, we concur with Ref. [39] that maximizing mission science return, in addition to understanding the true performance limits, suggests employing the GRS as the main sensor, in an isolated environment near the spacecraft center of mass.

Author Contributions: Conceptualization, W.J.W., D.B., P.B. and R.D.; validation, W.J.W., D.B., P.B., R.D. and S.V.; formal analysis, W.J.W. and G.C.; writing—original draft preparation, W.J.W.; writing—review and editing, W.J.W., D.B., P.B., G.C., R.D. and S.V. All authors have read and agreed to the published version of the manuscript.

Funding: This research received no external funding.

Data Availability Statement: Not applicable.

Conflicts of Interest: The authors declare no conflict of interest.

Appendix A. Extraction of Differential Gravitational Acceleration in a Simplified Geodesy Measurement with Two-Spacecraft and Reference Test Masses

We consider a simplified one-dimensional description of the geodesic measurement as an interferometric detection of the beatnote between transmitted and received laser beams at both SC, corrected for the non-inertial SC accelerations with local free-falling reference test masses (illustrated in the sketch of Figure A1). In our simplified, low velocity and single axis picture, the two SC are separated by a light time $T = \frac{L}{c}$ along axis x and exchange laser beams of nominal frequency ν.

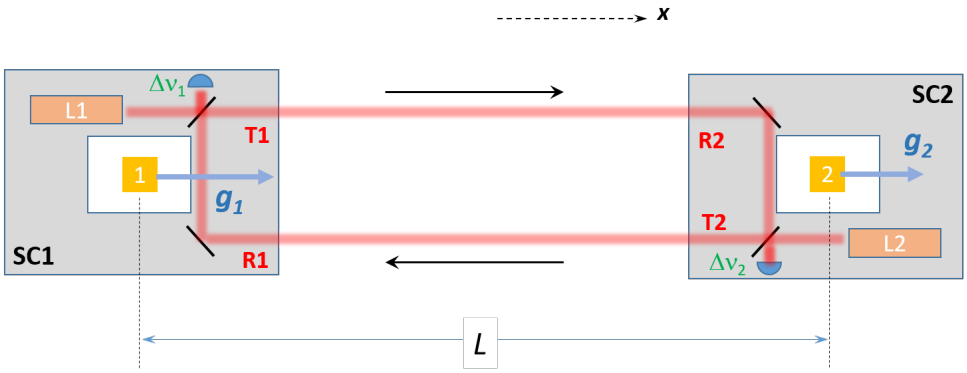

Figure A1. Cartoon of interspacecraft geodesy measurement configuration, including interspacecraft exchange of laser light, interferometric beatnote detection, and geodesic reference TM.

We define the beatnote measured at SC k, $\Delta\nu_k \equiv \nu_{Rk} - \nu_{Tk} + \nu_{nk}$, where ν_R is the frequency of the *R*eceived beam at SC k from the distant SC, ν_{Tk} is the locally *T*ransmitted beam from k and ν_{nk} is the noise in the SC k beatnote measurement, all in the reference frame of SC k. Considering the Doppler shift from the relative motion in the two SC

$$\begin{aligned} \Delta\nu_1(t) &\approx \nu_{T2}(t-T) - \nu_{T1}(t) + \nu_{n1}(t) \\ &+ \frac{\nu}{c}[\dot{x}_{SC1}(t) - \dot{x}_{SC2}(t-T)] \end{aligned} \tag{A1}$$

and

$$\begin{aligned} \Delta\nu_2(t-T) &\approx \nu_{T1}(t-2T) - \nu_{T2}(t-T) + \nu_{n2}(t-T) \\ &+ \frac{\nu}{c}[\dot{x}_{SC1}(t-2T) - \dot{x}_{SC2}(t-T)] \end{aligned} \tag{A2}$$

Summing the two measured beatnotes, we obtain an effective round trip (RT) beatnote,

$$\begin{aligned} \Delta\nu_{RT}(t) &\equiv \Delta\nu_1(t) + \Delta\nu_2(t-T) \\ &\approx \nu_{T1}(t-2T) - \nu_{T1}(t) \\ &\quad +\nu_{n1}(t) + \nu_{n2}(t-T) \\ &\quad +\frac{\nu}{c}[\dot{x}_{SC1}(t) + \dot{x}_{SC1}(t-2T) - 2\dot{x}_{SC2}(t-T)] \end{aligned} \tag{A3}$$

With proper timing (T) this calculated roundtrip beatnote is thus sensitive only to the frequency of the laser in SC1 (not in SC2) and is independent of possible laser servo control at SC2 (we simplify the notation for this one laser, $\nu_{T1} \equiv \nu_L$). We will neglect, $T \approx 0.7$ ms as very short compared to the measurement band and the dynamics of the relative SC motion, except where it enters linearly in the imperfect cancellation of the SC1 laser noise at times t and $(t-2T)$. We thus can approximate, for instance, $\dot{x}_{SC1}(t) + \dot{x}_{SC1}(t-2T) \approx 2\dot{x}_{SC1}(t)$. Taking an additional derivative and multiplying by $\frac{c}{2\nu}$ yields an expression for the differential SC acceleration,

$$\frac{c}{2}\frac{\Delta\dot{\nu}_{RT}(t)}{\nu} \approx \frac{c}{2\nu}[\dot{\nu}_{T1}(t-2T) - \dot{\nu}_{T1}(t)] + \frac{c}{2\nu}[\dot{\nu}_{n1} + \dot{\nu}_{n2}] + [\ddot{x}_{SC1} - \ddot{x}_{SC2}] \tag{A4}$$

This contains the differential gravity "science" signal in the relative acceleration between the distant SC, but including also any additional non-inertial "drag" accelerations acting on the two SC. The SC accelerations can be then be referred to the geodesic reference TM, with minimal or at least better modelled accelerations. We consider the local posi-

tion *M*easurement—x_{Mk}—of relative TM position (x_k) to SC motion—performed with a capacitive or local interferometric readout—considering measurement noise x_{nk},

$$\Delta x_{Mk} = x_k - x_{SCk} + x_{nk} \tag{A5}$$

Additionally, the equation of motion of the TM contains the desired gravitational acceleration (g_k) in addition to spurious accelerations (g_{nk}), any (known) commanded actuation forces g_{ck}, and the stiffness coupling to the SC motion, characterized by spring constant (per unit mass) ω^2_{xxk}

$$\ddot{x}_k = g_k + g_{nk} + g_{ck} - \omega^2_{xxk}(x_k - x_{SCk}) \tag{A6}$$

Combining Equations (A4), (A5) (double differentiated), and (A6) to substitute for the spacecraft acceleration $\ddot{x}_{SC}$, we obtain a geodesy observable for the difference in gravitational acceleration, constructed from measured data for the inter-SC interferometer, the two local TM readouts between the two TM,

$$\begin{aligned} \Delta\hat{g} \;&\equiv\; -\frac{c}{2}\frac{\Delta\dot{\nu}_{RT}}{\nu} - g_{c2} + g_{c1} + \ddot{x}_{M2} - \ddot{x}_{M1} + \omega^2_{xx2}x_{M2} - \omega^2_{xx1}x_{M1} \\ &\approx\; (g_2 - g_1) \\ &-\; \frac{c}{2\nu}(\dot{\nu}_{n1} + \dot{\nu}_{n2}) + \frac{c}{2\nu}[\dot{\nu}_L(t) - \dot{\nu}_L(t-2T)] + (g_{2n} - g_{1n}) + \left(\ddot{x}_{2n} + \omega^2_{xx2}x_{2n}\right) - \left(\ddot{x}_{1n} + \omega^2_{xx1}x_{1n}\right) \end{aligned} \tag{A7}$$

The first line indicates the calculation of the differential acceleration observable $\Delta\hat{g}$, which includes (line 2) the desired differential gravitational acceleration and the background (line 3) of noise effects.

In the absence of applied forces on the TM—$g_{ck} = 0$—this expression is valid for a single arm interferometric tidal acceleration measurement, for geodesy or for a single arm in a LISA "Michelson" combination. We note also that the actuation force and spacecraft coupling term (stiffness correction) are included in the calculation of the observable, using telemetry data for applied force commands and the local TM readout, as in LISA Pathfinder, requiring calibration knowledge for the actuator gain and stiffness [2,25]. We can also see how the residual noise related to spacecraft coupling is not the residual control jitter—$(x_{TM} - x_{SC})$—but rather the noise in the relative motion readout, x_{1n}, though a miscalibration of the relative displacement measurement can add noise proportional to the control jitter.

We can analyze the residual noise in the Fourier domain:

$$\Delta\tilde{g} = (\tilde{g}_{n2} - \tilde{g}_{n2}) + \frac{1}{2}\omega^2(\tilde{x}_{SC1} + \tilde{x}_{SC2}) - \omega^2 L\frac{\Delta\tilde{\nu}}{\nu} + \left[\left(-\omega^2 + \omega^2_{xx2}\right)\tilde{x}_{TM2}\right] + \left[\left(-\omega^2 + \omega^2_{xx1}\right)\tilde{x}_{TM1}\right] \tag{A8}$$

where $\frac{\Delta\nu}{\nu}$ is the laser relative intensity noise, x_{SCk} the effective error in the "1-way" measurement of the motion of SC k relative to the incoming beam—with a displacement to phase conversion $\delta x = \frac{c}{\nu}\frac{\delta\phi}{2\pi}$—and x_{TMk} represents the error in the TM k position readout relative to SC k.

Considering each TM and each position readout to have statistically equal and fully uncorrelated noise levels, we arrive to the differential acceleration noise breakdown shown in Equation (1).

We note that any baseline distorsion δx between the optical reference for the inter-spacecraft measurement and the GRS reference for the local TM measurement will enter, in Equations (1) and (A8) , as an effective contribution to the inter-spacecraft interferometry measurement. This thermal-mechanical contribution can be significant to the overall metrology noise at lower frequencies and is addressed with careful mechanical design, including "triple mirror assemblies" as mentioned in Refs. [7,10].

This idealized 1D description, as illustrated in Figure A1, indeed represents a simplified view of the entire geodesy measurement. It neglects the complications of spacecraft pointing and the inertial forces related to the spacecraft pointing noise, in addition to the

various terms of sensing and force-gradient cross coupling, which can impact performance in a significant way. Additionally relevant is the orbital determination in accurately converting the measured differential acceleration along a dynamically changing measurement axis into a gravitational measurement in Terrestrial coordinates. Still this 1D picture is useful to understand the fundamental limits in an "along track" differential acceleration measurement for geodesy.

References

1. Amaro-Seaone, P. Laser Interferometer Space Antenna: A proposal in Response to the ESA Call for L3 Mission Concepts. 2017. Available online: http://xxx.lanl.gov/abs/1702.00786 (accessed on 23 February 2017).
2. Armano, M.; Audley, H.; Auger, G.; Baird, J.T.; Bassan, M.; Binetruy, P.; Born, M.; Bortoluzzi, D.; Brandt, N.; Caleno, M.; et al. Sub-Femto-*g* Free Fall for Space-Based Gravitational Wave Observatories: LISA Pathfinder Results. *Phys. Rev. Lett.* **2016**, *116*, 231101. [CrossRef]
3. Armano, M.; Audley, H.; Baird, J.; Binetruy, P.; Born, M.; Bortoluzzi, D.; Castelli, E.; Cavalleri, A.; Cesarini, A.; Cruise, A.M.; et al. Beyond the Required LISA Free-Fall Performance: New LISA Pathfinder Results down to 20 μHz. *Phys. Rev. Lett.* **2018**, *120*, 061101. [CrossRef]
4. Weber, W.J.; Bortoluzzi, D.; Cavalleri, A.; Carbone, L.; Lio, M.D.; Dolesi, R.; Fontana, G.; Hoyle, C.D.; Hueller, M.; Vitale, S. Position sensor for flight testing of LISA drag-free control. In *Gravitational-Wave Detection*; SPIE: Bellingham, WA, USA, 2003; Volume 4856, pp. 31–42.
5. Dolesi, R.; Bortoluzzi, D.; Bosetti, P.; Carbone, L.; Cavalleri, A.; Cristofolini, I.; Da Lio, M.; Fontana, G.; Fontanari, V.; Foulon, B.; et al. Gravitational sensor for LISA and its technology demonstration mission. *Class. Quantum Grav.* **2003**, *20*, S99. [CrossRef]
6. Landerer, F.W.; Flechtner, F.M.; Save, H.; Webb, F.H.; Bandikova, T.; Bertiger, W.I.; Bettadpur, S.V.; Byun, S.H.; Dahle, C.; Dobslaw, H.; et al. Extending the Global Mass Change Data Record: GRACE Follow-on Instrument and Science Data Performance. *Geophys. Res. Lett.* **2020**, *47*, e2020GL088306. [CrossRef]
7. Abich, K.; Abramovici, A.; Amparan, B.; Baatzsch, A.; Okihiro, B.B.; Barr, D.C.; Bize, M.P.; Bogan, C.; Braxmaier, C.; Burke, M.J.; et al. In-Orbit Performance of the GRACE Follow-on Laser Ranging Interferometer. *Phys. Rev. Lett.* **2019**, *123*, 031101. [CrossRef]
8. Kang, K.; Bender, P.L. Improved measurements of short-period mass variations with future earth gravity missions. *J. Geophys. Res. Solid Earth* **2021**, *126*, e2020JB020720. [CrossRef]
9. Cristophe, B.; Boulanger, D.; Foulon, B.; Huynh, P.A.; Lebat, V.; Liorzou, F.; Perrot, E. A new generation of ultra-sensitive electrostatic accelerometers for GRACE Follow-on and towards the next generation gravity missions. *Acta Astronaut.* **2015**, *117*, 1–7. [CrossRef]
10. Alvarez, A.D.; Bevilacqua, R.; Hollis, H.; Mueller, G.; Knudston, A.; Patel, U.; Sanjuan, J.; Wass, P.; Conklin, J.W. A Simplified Gravitational Reference Sensor for Satellite Geodesy. 2021. Available online: http://xxx.lanl.gov/abs/2107.08545v4 (accessed on 12 January 2022).
11. Massotti, L.; Siemes, C.; March, G.; Haagmans, R.; Silvestrin, P. Next Generation Gravity Mission elements of the Mass Change and Geoscience International Constellation: From orbit selection to instrument and mission design. *Remote Sens.* **2021**, *13*, 3935. [CrossRef]
12. Behzadpour, S.; Mayer-Gürr, T.; Krauss, S. GRACE Follow-On Accelerometer Data Recovery. *J. Geophys. Res.* **2021**, *126*, e2020JB021297. [CrossRef]
13. Weber, W.J. Position sensors for LISA drag-free control. *Class. Quantum Grav.* **2002**, *19*, 1751. [CrossRef]
14. Heinzel, G.; Wand, V.; Danzmann, K. The LTP interferometer and phasemeter. *Class. Quantum Grav.* **2004**, *21*, S581. [CrossRef]
15. Zahnd, B.; Zimmermann, M.; Spörri, R. LISA Pathfinder cage and vent mechanism—development and qualification. In Proceedings of the 15th European Space Mechanisms and Tribology Symposium—ESMATS 2013, Noordwijk, The Netherlands, 25–27 September 2013.
16. Mäusli, P.A.; Neukom, A.; Romano, R.; Köker, I.; Durrant, S. Development of a Novel Piezo Actuated Release Mechanism. In Proceedings of the 12th European Space Mechanisms and Tribology Symposium—ESMATS, Liverpool, UK, 19–21 September 2007.
17. Sumner, T.; Araújo, H.; Davidge, D.; Howard, A.; Lee, C.; Rochester, G.; Shaul, D.; Wass, P. Description of charging/discharging processes of the LISA sensors. *Class. Quantum Grav.* **2004**, *21*, S597. [CrossRef]
18. Bortoluzzi, D.; Vignotto, D.; Zambotti, A.; Armano, M.; Audley, H.; Baird, J.; Binetruy, P.; Born, M.; Castelli, E.; Cavalleri, A.; et al. In-flight testing of the injection of the LISA Pathfinder test mass into a geodesic. *Adv. Space Res.* **2021**, *67*, 504. [CrossRef]
19. Armano, M.; Audley, H.; Auger, G.; Baird, J.; Binetruy, P.; Born, M.; Bortoluzzi, D.; Brandt, N.; Bursi, A.; Caleno, M.; et al. Constraints on LISA Pathfinder's self-gravity: Design requirements, estimates and testing procedures. *Class. Quantum Grav.* **2016**, *33*, 235015. [CrossRef]
20. Armano, M.; Audley, H.; Baird, J.; Binetruy, P.; Born, M.; Bortoluzzi, D.; Castelli, E.; Cavalleri, A.; Cesarini, A.; Cruise, A.M.; et al. Precision charge control for isolated free-falling test masses: LISA pathfinder results. *Phys. Rev. D* **2018**, *98*, 062001. [CrossRef]
21. Kenyon, S.P.; Letson, B.; Clark, M.; Olatunde, T.; Ritten, L.; Schindler, J.; Wass, P.J.; Conklin, J.W.; Barke, S.; Mueller, G.; et al. A Charge Management System for Gravitational Reference Sensors – Design and Instrument Testing. In Proceedings of the IEEE Aerospace Conference, Big Sky, MT, USA, 6–13 March 2021. [CrossRef]

22. Gan, L.; Mance, D.; Zweifel, P. LTP IS FEE Sensing Channel: Front-End Modeling and Symmetry Adjustment Method. *IEEE Sens. J.* **2011**, *12*, 1071. [CrossRef]
23. Armano, M.; Audley, H.; Auger, G.; Baird, J.; Bassan, M.; Binetruy, P.; Born, M.; Bortoluzzi, D.; Brandt, N.; Caleno, M.; et al. Capacitive sensing of test mass motion with nanometer precision over millimeter-wide sensing gaps for space-borne gravitational reference sensors. *Phys. Rev. D* **2017**, *96*, 062004. [CrossRef]
24. Armano, M.; Audley, H.; Baird, J.; Born, M.; Bortoluzzi, D.; Cardines, N.; Castelli, E.; Cavalleri, A.; Cesarini, A.; Cruise, A.M.; et al. Analysis of the accuracy of actuation electronics in the Laser Interferometer Space Antenna Pathfinder. *Rev. Sci. Instrum.* **2020**, *91*, 045003. [CrossRef]
25. Armano, M.; Audley, H.; Baird, J.; Binetruy, P.; Born, M.; Bortoluzzi, D.; Castelli, E.; Cavalleri, A.; Cesarini, A.; Cruise, A.M.; et al. Calibrating the system dynamics of LISA Pathfinder. *Phys. Rev. D* **2018**, *97*, 122002. [CrossRef]
26. Antonucci, F.; Armano, M.; Audley, H.; Auger, G.; Benedetti, M.; Binetruy, P.; Boatella, C.; Bogenstahl, J.; Bortoluzzi, D.; Bosetti, P.; et al. From laboratory experiments to LISA Pathfinder: Achieving LISA geodesic motion. *Class. Quantum Grav.* **2011**, *28*, 094002. [CrossRef]
27. Armano, M.; Audley, H.; Auger, G.; Baird, J.T.; Binetruy, P.; Born, M.; Bortoluzzi, D.; Brandt, N.; Bursi, A.; Caleno, M.; et al. Charge-Induced Force Noise on Free-Falling Test Masses: Results from LISA Pathfinder. *Phys. Rev. Lett.* **2017**, *118*, 171101. [CrossRef] [PubMed]
28. Speake, C.C. Forces and force gradients due to patch fields and contact-potential differences. *Class. Quantum Grav.* **1996**, *12*, A291. [CrossRef]
29. Antonucci, F.; Cavalleri, A.; Dolesi, R.; Hueller, M.; Nicolodi, D.; Tu, H.B.; Vitale, S.; Weber, W.J. Interaction between Stray Electrostatic Fields and a Charged Free-Falling Test Mass. *Phys. Rev. Lett.* **2012**, *108*, 181101. [CrossRef]
30. Shaul, D.N.A.; Araújo, H.M.; Rochester, G.K.; Sumner, T.J.; Wass, P.J. Evaluation of disturbances due to test mass charging for LISA. *Class. Quantum Grav.* **2005**, *22*, S297. [CrossRef]
31. Sumner, T.; Mueller, G.; Conklin, J.W.; Wass, P.J.; Hollington, D. Charge induced acceleration noise in the LISA gravitational reference sensor. *Class. Quantum Grav.* **2020**, *37*, 4. [CrossRef]
32. Cavalleri, A.; Ciani, G.; Dolesi, R.; Heptonstall, A.; Hueller, M.; Nicolodi, D.; Rowan, S.; Tombolato, D.; Vitale, S.; Wass, P.J.; et al. Increased Brownian Force Noise from Molecular Impacts in a Constrained Volume. *Phys. Rev. Lett.* **2009**, *103*, 140601. [CrossRef]
33. Mehta, P.M.; Walker, A.C.; Sutton, E.K.; Godinez, H.C. New density estimates derived using accelerometers on board the CHAMP and GRACE satellites. *Space Weather* **2017**, *15*, 558. [CrossRef]
34. Armano, M.; Audley, H.; Baird, J.; Binetruy, P.; Born, M.; Bortoluzzi, D.; Castelli, E.; Cavalleri, A.; Cesarini, A.; Cruise, A.M.; et al. Spacecraft and interplanetary contributions to the magnetic environment on-board LISA Pathfinder. *Mon. Not. R. Astron. Soc.* **2020**, *494*, 3014. [CrossRef]
35. Armano, M.; Audley, H.; Baird, J.; Binetruy, P.; Born, M.; Bortoluzzi, D.; Castelli, E.; Cavalleri, A.; Cesarini, A.; Cruise, A.M.; et al. Temperature stability in the sub-milliHertz band with LISA Pathfinder. *Mon. Not. R. Astron. Soc.* **2019**, *486*, 3368. [CrossRef]
36. Carbone, L.; Cavalleri, A.; Ciani, G.; Dolesi, R.; Hueller, M.; Tombolato, D.; Vitale, S.; Weber, W.J. Thermal gradient-induced forces on geodesic reference masses for LISA. *Phys. Rev. D* **2007**, *76*, 102003. [CrossRef]
37. Cavalleri, A.; Ciani, G.; Dolesi, R.; Hueller, M.; Nicolodi, D.; Tombolato, D.; Wass, P.J.; Weber, W.J.; Vitale, S.; Carbone, L. Direct force measurements for testing the LISA Pathfinder gravitational reference sensor. *Class. Quantum Grav.* **2009**, *26*, 094012. [CrossRef]
38. Ciani, G.; Chilton, A.; Apple, S.; Olatunde, T.; Aitken, M.; Mueller, G.; Conklin, J.W. A new torsion pendulum for gravitational reference sensor technology development. *Rev. Sci. Instrum.* **2017**, *88*, 064502. [CrossRef] [PubMed]
39. Bender, P.L. An improved Next Generation Gravity Mission. *Remote Sens.* **2021**, *14*, 948. [CrossRef]